JOURNAL OF VIROLOGY, Apr. 2003, p. 4528–4538 Vol. 77, No. 8
0022-538X/03/$08.00+0 DOI: 10.1128/JVI.77.8.4528–4538.2003

Switching Species Tropism: an Effective Way To Manipulate the Feline Coronavirus Genome

Bert Jan Haijema, Haukeliene Volders, and Peter J. M. Rottier*

Institute of Virology, Department of Infectious Diseases and Immunology, Faculty of Veterinary Medicine, Utrecht University, 3584 CL Utrecht, The Netherlands

Received 29 August 2002/Accepted 21 January 2003

Feline infectious peritonitis virus (FIPV), a coronavirus, is the causative agent of an invariably lethal infection in cats. Like other coronaviruses, FIPV contains an extremely large positive-strand RNA genome of ca. 30 kb. We describe here the development and use of a reverse genetics strategy for FIPV based on targeted RNA recombination that is analogous to what has been described for the mouse hepatitis virus (MHV) (L. Kuo et al., J. Virol. 74:1393-1406, 2000). In this two-step process, we first constructed by targeted recombination a mutant of FIPV, designated mFIPV, in which the ectodomain of the spike glycoprotein was replaced by that of MHV. This switch allowed for the selection of the recombinant virus in murine cells: mFIPV grows to high titers in these cells but has lost the ability to grow in feline cells. In a second, reverse process, mFIPV was used as the recipient, and the reintroduction of the FIPV spike now allowed for selection of candidate recombinants by their regained ability to grow in feline cells. In this fashion, we reconstructed a wild-type recombinant virus (r-wtFIPV) and generated a directed mutant FIPV in which the initiation codon of the nonstructural gene 7b had been disrupted (FIPVΔ7b). The r-wtFIPV was indistinguishable from its parental virus FIPV 79-1146 not only for its growth characteristics in tissue culture but also in cats, exhibiting a highly lethal phenotype. FIPVΔ7b had lost the expression of its 7b gene but grew unimpaired in cell culture, confirming that the 7b glycoprotein is not required in vitro. We establish the second targeted RNA recombination system for coronaviruses and provide a powerful tool for the genetic engineering of the FIPV genome.

Feline infectious peritonitis (FIP) is a progressive, usually lethal disease of cats caused by a coronavirus, the FIP virus (FIPV). Coronaviruses are enveloped viruses infecting numerous mammalian and avian species. They are spherical viruses that contain a basic set of four essential structural proteins: the membrane (M) protein, the small envelope (E) protein, the spike (S) glycoprotein, and the nucleocapsid (N) protein. The N protein wraps the genomic RNA into a nucleocapsid that is surrounded by a lipid membrane in which the S, M, and E proteins occur. The M and E proteins are essential and sufficient for viral envelope formation (48). The M protein also interacts with the N protein, presumably to mediate the assembly of the nucleocapsid into the virion (13, 23, 34). Trimers of the S protein (11) form the characteristic spikes that protrude from the virion membrane. The S protein is responsible for viral attachment to specific host cell receptors—the basis of these viruses' narrow host range specificity—and for cell-cell fusion (for a review, see reference 3).

The coronaviral genome is a capped, polyadenylated, nonsegmented, infectious, positive-strand RNA molecule of ca. 30 kb, the largest of all known viral RNA genomes (Fig. 1). Its 5′ two-thirds are occupied by genes open reading frame (ORF) 1a and ORF 1b, which are translated from infecting genomic RNA into two polyprotein precursors from which the viral replication and transcription functions are derived. Downstream of ORF 1b a number of genes occur that encode the structural and several nonstructural proteins. These genes are expressed through a 3′-coterminal nested set of subgenomic mRNAs that are synthesized by a process of discontinuous transcription. The subgenomic mRNAs represent variable lengths of the 3′ end of the viral genome, each one provided at its 5′ end with a sequence identical to the genomic 5′ "leader" sequence (for reviews, see references 12 and 47). The mRNAs are each functionally monocistronic: proteins are translated only from the 5′-most ORF.

FIP is an immunopathogenic disease. The infection causes lesions in many organs, most prominently in the liver and spleen (7). The disease is further characterized by disseminated perivascular pyogranulomatous inflammation and exudative fibrinous serositis in the abdominal and thoracic cavities. In addition to this "wet" or effusive form, a "dry" or noneffusive form of FIP also occurs. Both forms are different manifestations of the same infection. Despite many studies, the pathogenesis of FIP is still not well understood. As for other coronaviruses, the lack of reverse genetics systems has severely hampered the study of FIPV biology and pathogenesis.

Until very recently, coronavirus manipulation was only possible with a murine virus, the mouse hepatitis virus (MHV), due mainly to pioneering work in the laboratory of P. Masters, who used RNA recombination to introduce changes into the viral genome (28). Because of their huge genomic size, infectious cDNA clones of transmissible gastroenteritis virus (TGEV) (1, 51), human coronavirus (HuCV) (46), infectious bronchitis virus (IBV) (2), and murine hepatitis virus (MHV) (52) were only obtained recently using different creative approaches.

We describe here the development of a reverse genetics system for FIPV. The system is based on targeted RNA recombination, making use of a newly developed strategy for

* Corresponding author. Mailing address: Institute of Virology, Faculty of Veterinary Medicine, Utrecht University, P.O. Box 80.165, 3508 TD Utrecht, The Netherlands. Phone: 31-30-2532462. Fax: 31-30-2536723. E-mail: P.Rottier@vet.uu.nl.

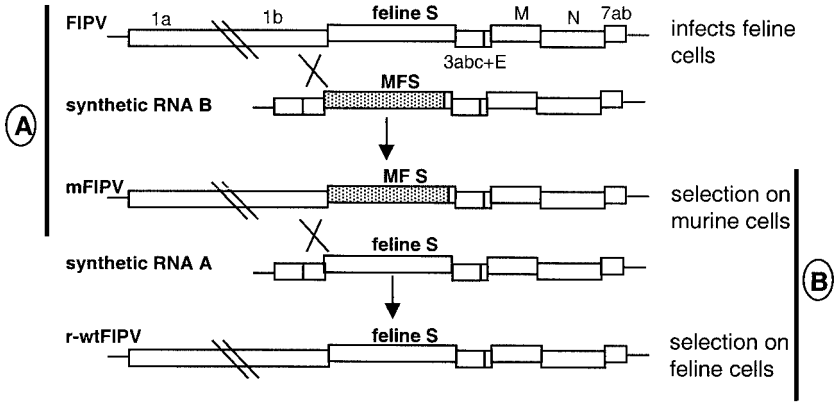

FIG. 1. Overview of the targeted recombination strategy for FIPV. The scheme shows the construction of mFIPV (A) and r-wtFIPV (B) by targeted recombination between FIPV 79-1146 and synthetic donor RNA B and between mFIPV and synthetic donor RNA A, respectively. A single crossover event anywhere within the 3′ domain of the ORF 1b gene present in the donor RNA (indicated by a cross) generates a recombinant genome. In the first step (section A), the recombinant mFIPV acquires the ectodomain-encoding region of the MHV S gene (dotted); in the second step (section B), r-wtFIPV regains the feline S gene. mFIPV should lose the ability to infect feline cells and simultaneously gain the ability to infect murine cells and vice versa for r-wtFIPV.

recombinant virus selection (22). The key feature of the method is an interspecies chimeric MHV that serves as the recipient. This virus, designated fMHV and itself generated by targeted recombination, carries a chimeric spike protein of which the ectodomain is derived from FIPV. As a result, fMHV infects feline but not murine cells. When synthetic RNA carrying the wild-type MHV S gene is transfected into fMHV-infected cells, recombinant viruses that acquired this gene can simply be selected by growth in murine cells. This allows the mutagenesis of all MHV genes downstream of ORF 1b. We describe here how similar principles were successfully applied to establish a strategy for the genetic engineering of the subgroup 1 coronavirus, FIPV.

MATERIALS AND METHODS

Viruses, cells, and antibodies. *Felis catus* whole fetus (FCWF) cells cells (American Type Culture Collection) were used to propagate, select, plaque assay, or radiolabel FIPV strain 79-1146 (30), wild-type recombinant virus (r-wtFIPV), and FIPVΔ7B. Mouse LR7 (22) cells were used to propagate MHV strain A59 and mutant FIPV (mFIPV). Both LR7 and FCWF cells were maintained as monolayer cultures in Dulbecco modified Eagle medium containing 10% fetal calf serum, 100 IU of penicillin/ml, and 100 μg of streptomycin/ml (all from Life Technologies, Ltd., Paisley, United Kingdom).

Ascites G73 from an FIPV-infected cat was provided by H. Vennema. The rabbit antiserum K134 raised against purified MHV strain A59 has been described elsewhere (43). Monoclonal antibody (MAb) WA3.10 directed against an epitope present in the MHV S ectodomain was obtained from J. Fleming (University of Wisconsin, Madison, Wis.) and MAb 23F4.5, which recognizes an epitope in the ectodomain of the S protein of FIPV 79-1146 (38), was provided by Rhône Mérieux (Lyon, France).

Plasmid constructions. (i) Construction of donor RNA transcription vector pBRDI1 and derivatives. A cDNA clone comprising the 5′ end of FIPV 79-1146 was obtained by reverse transcription-PCR (RT-PCR) with genomic viral RNA isolated from virions as a template and PR238 and PR898 as plus- and minus-strand primers, respectively, yielding the 716-bp fragment 1 (small boxed region in Fig. 2A). Primer PR898 contains an additional *Sac*I restriction site shown in bold in Table 1. A double-stranded linker (PRT7; Table 1 and see also Fig. 2) encoding a T7 polymerase recognition site (underlined, Table 1), as well as an additional *Xho*I restriction site (in boldface in Table 1), was ligated to fragment 1, resulting in fragment 2 (see Fig. 2B, part I, for the nucleotide sequence around the fusion site of the T7 promoter and 5′ end of FIPV cDNA). Fragment 3 (2,275 bp) was generated by PCR with primers PR897 and PR238 and cDNA 1B1 as a template. Clones 1B1, 2B11, and 2E7 are FIPV 79-1146-derived cDNA clones ligated into pUC8 (5, 6). To fuse fragments 2 and 3, splicing overlap extension PCR (SOE-PCR) was employed, using the overlap between the two fragments through primers PR898 and PR897, followed by amplification with primers PRT7 and PR238. This resulted in the 2,989-bp fragment 4, introducing a unique *Sac*I restriction site at the fusion site (see Fig. 2B, part II, for the nucleotide sequence around the fusion site). Fragment 4 encodes a fusion protein (248 amino acids [aa]) composed of the N-terminal 127 aa of ORF 1a and the C-terminal 121 aa of ORF 1b (see Fig. 2B, part II, for the sequence around the fusion site). Fragment 4 was cloned into pGEMT-Easy, its integrity was verified by sequencing, and it was subsequently cloned as a 2.7-kb *Xho*I-*Hin*dIII fragment into *Xho*I-*Hin*dIII-digested pBRXN (16), resulting in pBRXN1. Next, a 2.8-kb *Hin*dIII-*Bam*HI fragment derived from cDNA 1B1 was isolated and ligated into *Hin*dIII-*Bam*HI-digested pBRXN1, resulting in pBRXN2. pBRXN3 was constructed as follows: a 3.5-kb *AlfII-Bam*HI fragment isolated from cDNA 2B11 was ligated into *Alf*II-*Bam*HI-digested pBRXN2. A cDNA clone of the 3′ end of FIPV 79-1146 was obtained by RT-PCR with genomic viral RNA isolated from virions as a template and PR302 and PR301 as plus- and minus-strand primers, respectively, resulting in the 305-bp fragment 5. Primer PR301 contains an added *Not*I restriction site downstream of the poly(A) tail of 20 bases (Table 1 [in boldface]) to facilitate runoff T7 transcription. Fragment 5 was ligated into pGEMT-Easy, verified by DNA sequencing, and cloned as a 0.3-kb *Pml*I-*Bam*HI fragment into *Pml*I-*Bam*H-digested 2E7, resulting in 2E7polyA. A 2.5-kb *Sna*BI-*Bam*HI fragment was isolated from 2E7polyA and ligated into *Sna*BI-*Bam*HI-digested pBRXN3, resulting in the donor RNA transcription vector pBRDI1. Mutations in the start codon of gene 7b were introduced by SOE-PCR. Combinations of primers PR1248 and PR1329 and primers PR1328 and PR301 were used to generate fragments of 1,547 bp (fragment A) and 944 bp (fragment B), respectively. Fragments A and B were fused by using the overlap between both fragments with primers PR1329 and PR1328, followed by amplification with primers PR1248 and PR301, yielding the 2,452-bp fragment C. Fragment C was digested with *Mlu*I and *Not*I and cloned into *Mlu*I- and *Not*I-digested pBRDI1, resulting in pBRDI1ΔATG7b.

An out-of-frame deletion in the nucleocapsid gene was constructed by digesting plasmid pBRDI1 with *Mlu*I, treating it with Klenow enzyme, and finally religating the blunt-ended plasmid, yielding pBRDI1ΔMluI.

(ii) Construction of donor RNA transcription vector pBRDI2. To fuse the 3′ end of the ORF 1b gene to the 5′ end of the MHV S gene, SOE-PCR was applied by using combinations of primers PR897 and PR1000 and primers PR1003 and PR901 with pBRDI1 and pTMFS (17) as templates, yielding the 357- and 1,175-bp fragments 6 and 7, respectively (Fig. 2). These fragments were fused by using their overlap through primers PR1000 and PR1003 and amplified with primers PR897 and PR901, resulting in the 1,511-bp fragment 8. Fragment 8 was ligated into *Sac*I-*Stu*I-digested pTMFS as a 0.5-kb *Sac*I-*Stu*I fragment, resulting in pTMFS1. After partial and complete digestion of pTMFS1 with *Alf*II and with *Sac*I, respectively, a 4.8-kb *Sac*I-*Alf*II fragment encoding the C-terminal end of

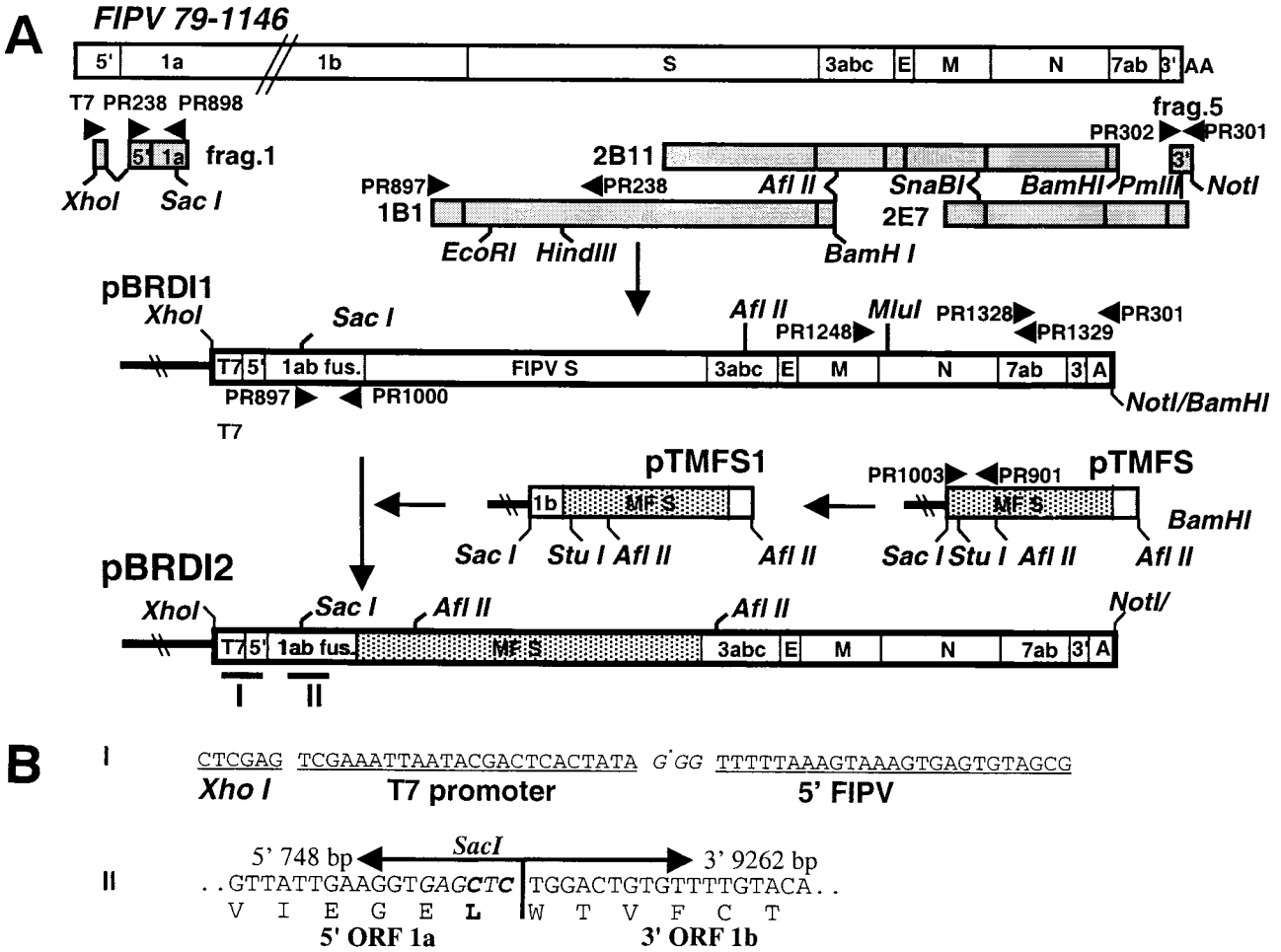

FIG. 2. Construction and composition of the transcription vectors pBRDI1 and pBRDI2, the templates for the synthetic donor RNA fragments A and B, respectively. (A) Shown at the top is a schematic representation of the FIPV 79-1146 genome. The shaded bars represent the various FIPV cDNA clones used to assemble pBRDI1. For details, see Materials and Methods. Small arrows indicate the primers (see Table 1 for primer numbers, sequences, and locations) used to generate the various fragments (see Materials and Methods). The dotted bars represent sequences encoding the MHV S ectodomain (pTMFS and pTMFS1 are not drawn to scale). The broad line at the left of each vector indicates pBRXN vector sequences. T7, 5′, 3′, and A indicate the T7 RNA polymerase transcription promoter sequence, the 5′- and 3′-untranslated region sequences, and a polyadenylate segment, respectively. Restriction sites relevant to plasmid construction are shown. (B) Some sequences are specified: I, the T7 promoter sequence preceded by a *Xho*I restriction sequence and followed by the sequence of the 5′-terminal region; the transcriptional start is indicated by an asterisk; and II, the in-frame transition of the 5′ ORF 1a and the 3′ ORF 1b sequences. Base pairs changed to create an unique *Sac*I restriction site are in italics and in boldface. Below the nucleotide sequence the amino acid sequence is shown, with the residues that were changed due to the introduction of the *Sac*I site indicated in boldface.

ORF 1b and the entire S protein was isolated and cloned into *Sac*I-*Alf*II-digested pBRDI1, resulting in the donor RNA transcription vector pBRDI2.

Targeted recombination. A chimeric MHV-FIPV S (MF-S) gene was introduced into the FIPV genome by targeted RNA recombination between the synthetic donor RNA B and the recipient FIPV 79-1146 genome essentially as described previously (22). Capped, runoff donor RNA transcripts were synthesized from *Not*I-linearized pBRDI2 with a T7 polymerase kit (Ambion) as specified by the manufacturer. Donor RNA was electroporated (Gene Pulser electroporation apparatus [Bio-Rad]; two consecutive pulses of 0.3 kV/975 μF) into FIPV-infected (multiplicity of infection [MOI] of 0.4) FCWF cells (2×10^7 cells) at 4 h postinfection (p.i.). The electroporated cells were cocultured in a 25-cm^2 flask with 5×10^6 murine LR7 cells. Controls, originating from FIPV 79-1146-infected FCWF cells that had been mock transfected or from mock-infected cells that had been transfected with RNA B, were treated identically. After 48 h of incubation at 37°C, when syncytia could be detected in the murine LR7 cells, progeny virus in the culture supernatant was harvested, and candidate recombinants (i.e., mFIPV) were selected and purified by three consecutive cycles of endpoint dilution on LR7 cells at 37°C.

The construction of FIPV recombinants that had regained the FIPV S gene was carried out in a reverse process by using pBRDI1-derived donor RNAs and mFIPV as the recipient virus. Capped, runoff transcripts were synthesized from *Not*I-linearized pBRDI1, pBRDI1Δ7b, and pBRDI1ΔMluI, respectively, with a T7 RNA polymerase kit (Ambion) as specified by the manufacturer. The donor transcripts were electroporated (as specified above but applying two consecutive pulses of 0.85 kV/50 μF) into murine LR7 cells (2×10^7 cells) that had been infected 4 h earlier with mFIPV (MOI = 0.2). The electroporated cells were cocultured in a 25-cm^2 flask with 5×10^6 feline FCWF cells. After 24 h of incubation at 37°C, when massive syncytia were visible in the feline FCWF cells, progeny virus in the culture supernatant was harvested, and candidate recombinants were purified by two rounds of plaque purification on FCWF cells.

Genomic analysis of candidate recombinants. After plaque purification, monolayers (25 cm^2) of LR7 or FCWF cells were infected with the candidate recombinants, culture media were harvested at 24 h p.i., and viral RNA was isolated by using a QIAamp viral RNA Mini Kit (Qiagen) as specified by the manufacturer. The viral RNA was reverse transcribed under standard conditions by using Moloney murine leukemia virus reverse transcriptase (Gibco-BRL) with

TABLE 1. Primers

Primer[a]	Location (nucleotides)	Sense	Sequence
PRT7	1–33	+	5′-GATC***CTCGAG***TCGAAATTAATACGACTCACTATAGGG-3′
PR238	34–56	+	5′-TTTTTAAAGTAAAGTGAGTGTAG-3′
PR898	714–752	−	5′-***GAGCTC***ACCTTCAATAACTG-3′
PR897	716–752	+	5′-CAGTTATTGAAGGTGAGCTCTGGACTGTGTTTTGTAC-3′
PR238	2971–2989	−	5′-CAATTAGCACCAACAGG-3′
PR987	7637–7672	−	5′-GACGCGTTGTCCCTGTGTGGCCATTTGAAAGTTTAG-3′
PR301	9978–10020	−	5′-***GCGGCCGC***TTTTTTTTTTTTTTTTTTTTTGTGTATCACTATC-3′
PR302	9715–9737	+	5′-AACTAGTAAGGCAACCCGATGTCTAAAAC-3′
PR1248	7568–7587	+	5′-GGTGATTACTCAACAGAAGC-3′
PR1251	8766–8786	−	5′-GCGATCAGTTCGTAACCTC-3′
PR1328	9078–9115	+	5′-GGTGCATTATTTTAA***CACGTG***ATTGTTGTAATCCTTG-3′
PR1329	9076–9094	−	5′-TGTTAAAATAATGCACC-3′
PR1295	9723–9742	−	5′-GACCAGTTTTAGACATCG-3′
PR76	8169–8189	+	5′-CTCAATCTAGAGGAAGACACC-3′
PR1000	1052–1073	−	5′-CATGGCACATTAACTAAATG-3′
PR1003[A]	1054–1089	+	5′-CATTTAGTTAATGTGCCATGCTGTTCGTGTTTATTC-3′
PR901[A]	2208–2227	−	5′-CCAAAGCACCTGCCATAC-3′
PR990[A]	4713–4733	+	5′-CCTGATTTATCTCTCGATTTC-3′
PR1254	927–944	+	5′-GTGCCTTGTAACAATGC-3′
PR1255[A]	5662–5686	−	5′-CCAGTAAGCAATAATGTGG-3′
PR311	1250–1270	−	5′-CGGTACAAAGCCAAAAATGATAC-3′

[a] The location of primers is given relative to the nucleotide sequence of pBRDI1, except when the primer is marked with a superscript "A" (pBRDI2).

primer PR987 (mFIPV) or PR301 (r-wtFIPV, FIPVΔ7b, and FIPVΔMlu). cDNA was amplified by PCR with various primer pairs to characterize candidate recombinants. PCR amplifications were run for 30 cycles of 1 min at 94°C, 1 min at 48°C, and 2 min at 72°C with AmpliTaq DNA polymerase (Perlin-Elmer). Products were analyzed by agarose gel electrophoresis; in some cases, fragments were additionally purified from the gel, treated with appropriate restriction enzyme, and analyzed again by gel electrophoresis.

Radiolabeling and immunoprecipitation analysis of intracellular proteins. Confluent monolayers of FCWF cells or LR7 cells in 10-cm^2 tissue culture dishes were inoculated with virus (MOI = 10). At 4.5 h p.i., cells were washed with phosphate-buffered saline (PBS) and starved for 30 min in cysteine- and methionine-free modified Eagle medium containing 10 mM HEPES (pH 7.2) and 5% dialyzed fetal calf serum. The medium was then replaced with 600 μl of similar medium containing 100 μCi of ^{35}S In Vitro Cell-Labeling Mixture (Amersham), and cells were labeled for 2 h. Proteins were immunoprecipitated from cell lysates as described earlier (22). The immune complexes adsorbed to Pansorbin cells (Calbiochem) were incubated overnight at 4°C and were subsequently collected by low-speed centrifugation. Pellets were washed three times by resuspension and centrifugation. The final pellets were resuspended in electrophoresis sample buffer. The immunoprecipitates were analyzed by sodium dodecyl sulfate-polyacrylamide gel electrophoresis in 12.5% gels.

Immunofluorescence. LR7 cells and FCWF cells grown on coverslips in 35-mm culture dishes were inoculated with MHV, mFIPV, or FIPV (MOI = 0.5). After 1 h, the cells were washed with PBS and incubated in culture medium. At 6 h p.i., the cells were rinsed with PBS and fixed with precooled (−20°C) methanol for 10 min at −20°C. The cells were washed three times with PBS and incubated with various antibodies. After 30 min at room temperature, the cells were rinsed three times with PBS and stained with a corresponding fluorescein isothiocyanate-conjugated immunoglobulin G antibody (Cappel). Finally, the cells were washed three times with PBS and mounted in Fluorsave reagent (Calbiochem). Fluorescence was viewed with a confocal laser-scanning microscope.

Virulence assays. To study the virulence of FIPV 79-1146 and r-wtFIPV, an infection study was performed with healthy, female, specific-pathogen-free HsdCpd:CAD(BR) kittens (Harlan Sprague-Dawley, Inc.). At the start of the experiment the kittens were ca. 20 weeks old. Kittens were placed in two groups (four and five animals); the animals were inoculated oronasally with FIPV 79-1146 or r-wtFIPV (100 PFU/kitten). The two groups were housed separately in a closed facility. Kittens were examined for signs of disease or death on a daily basis for up to 3 months p.i. To avoid unnecessary suffering, kittens were euthanized once they had entered the irreversible terminal phase of FIP, as judged by the animal experts of the veterinary facility, and a full postmortem examination was performed. The approval of the Ethical Committee of the Utrecht University had been obtained for the animal experiments.

Nucleotide sequence accession numbers. The GenBank accession numbers for the nucleotide sequences of plasmids pBRDI1 and pBRDI2 are AY204704 and AY204705, respectively.

RESULTS

Construction of the donor RNA transcription vectors. The targeted RNA recombination experiments (Fig. 1) were carried out with synthetic donor RNA A and RNA B, which were transcribed from the transcription vectors pBRDI1 and pBRDI2 (Fig. 2), respectively. Plasmid pBRDI1 basically represents a pBR322 vector with an FIPV genomic cDNA lacking most of the polymerase gene sequences (for construction details, see Materials and Methods). The transcription vector pBRDI2 is similar to pBRDI1 but contains a hybrid spike gene (MF-S) instead of the FIPV spike. The hybrid spike gene is derived from pTMFS (17) and encodes a chimeric S protein: the 1,244-aa ectodomain is derived from MHV S, whereas the transmembrane and cytoplasmic tail (64 aa) are from FIPV S. The MF S protein was shown to be functional, causing syncytia in murine LR7 cells and being incorporated into FIPV virus-like particles when expressed together with the FIPV M and E proteins (17). To facilitate the efficient in vitro RNA transcription of synthetic donor RNAs, a T7 promoter sequence was placed immediately in front the FIPV cDNA sequences.

Generation of mFIPV. To obtain FIPV recombinants carrying a hybrid MF-S gene, donor RNA B transcribed in vitro from pBRDI2 was transfected into feline FCWF cells that had been infected with FIPV 79-1146. The infected and transfected FCWF cells were then cocultured with murine LR7 cells to allow the propagation of recombinant viruses that had acquired the ability to grow on murine cell as a consequence of a recombination event between the FIPV genome and the synthetic RNA B upstream of the S gene, resulting in mFIPV (Fig. 1A). After 48 h, LR7 cells exhibited syncytia only when cocultured with FCWF cells that had been both infected with

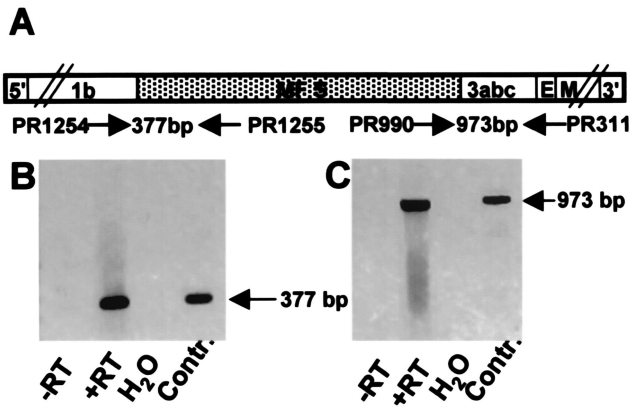

FIG. 3. RT-PCR analysis of recombinant mFIPV. RT-PCR was used to amplify the FIPV-MF S boundaries with RNA isolated from cells infected with mFIPV as a template. (A) Physical map of the genome of the mFIPV recombinant. The dotted area indicates the MF-S gene. The location of the primers used is indicated with an arrow, together with the expected size of the PCR products. (B) RT-PCR with primers PR1254 and PR1255. (C) RT-PCR with primers PR-990 and PR311. See Table 1 for primer sequences. Lanes −RT, no reverse transcriptase added; lanes +RT, reverse transcriptase added; lanes H_2O, H_2O replacing the template; lanes Contr., pBRDI2 used as a template.

FIPV and transfected with RNA B, indicating the dependence on the intended recombination. Thus, no LR7 syncytia were observed after coculture with nontransfected FIPV-infected FCWF cells or when the FCWF cells had been transfected but not infected. Candidate recombinant viruses present in the culture medium of the infected cells plus the transfected cells were purified from the pool of wild-type FIPV by selection on LR7 cells. Since the recombinant viruses failed to produce clear plaques on these cells, they were purified by three consecutive rounds of endpoint dilution. Several recombinant viruses, designated mFIPV, were thus isolated; all of these grew to a similar titer. One candidate mFIPV recombinant was selected for further characterization, and a high-titer stock was grown on murine LR7 cells.

Genetic analysis of the recombinant mFIPV. To test whether the candidate mFIPV recombinant had the intended genetic makeup, RT-PCR was performed on its genomic viral RNA by amplifying the hybrid S boundaries. The primers used and the DNA sizes expected are indicated in Fig. 3A. To verify the engineered upstream boundary between the ORF 1b gene and the MF-S gene, the FIPV-specific primer PR1254 and the MHV-specific primer PR1255 were used. A PCR product with the expected size of 377 bp (Fig. 3B, lane 2, arrow) was obtained when genomic RNA from mFIPV but not from FIPV or MHV (data not shown) was used as a template. The presence of the downstream boundary between the murine and feline S sequences of MF S was confirmed with the MHV S-specific primer PR990 and the FIPV-specific primer PR311. A PCR product with the expected size of 973 bp was observed (Fig. 3C, lane 2, arrow) only with genomic RNA from mFIPV as the template. Again, no PCR products were observed when FIPV or MHV RNA was used as a template (data not shown) or when either reverse transcriptase or template was omitted from the reaction (Fig. 3C, lanes 1 and 4, respectively). These results indicate that mFIPV has the projected chimeric genome composed of an FIPV backbone in which part of the S gene was replaced by that of MHV S.

To investigate whether the engineered boundaries had accumulated mutations during endpoint dilution purification and subsequent passaging, both the upstream (Fig. 3B, lane 2) and the downstream (Fig. 3C, lane 2) PCR fragments were cloned and sequenced. The results showed the DNA sequences of both fragments to be identical to the corresponding sequences in pBRDI2, indicating that no mutations had been acquired in these regions. Mutations elsewhere in the genome cannot, of course, be excluded. Obviously, the replacement of the S gene fragment was well tolerated.

Analysis of the mFIPV proteins. To further verify the identity of mFIPV, we characterized the candidate recombinant mFIPV at the protein level, in particular with respect to its S protein. For this purpose, murine LR7 cells were infected with mFIPV and the proteins were labeled with ^{35}S-labeled amino acids. As controls, LR7 and FCWF cells were infected with MHV and FIPV, respectively, and labeled similarly. After the labeling, cell lysates were prepared, and immunoprecipitations were carried out as described previously (22) with the following antibodies: G73 (αFIPV), an ascitic fluid from an FIPV-infected cat; K134 (αMHV), a rabbit serum raised against purified MHV strain A59; WA3.10 (αS_m), an MAb against an epitope present in the MHV S ectodomain; and 23F4.5 (αS_f), an MAb against an epitope in the FIPV S ectodomain. The electrophoretic patterns are shown in Fig. 4A. As expected, the G73 anti-FIPV antibodies precipitated the FIPV proteins S, M, and N (lane 10) but not the MHV proteins (lane 1). Also, the 23F4.5 MAb precipitated the feline S of FIPV (lane 11) but not the murine S of MHV (lane 2). The anti-MHV serum precipitated the MHV proteins S, N, and M (lane 3 and 4) but not the FIPV proteins (lane 12). The differences between the patterns in lanes 3 and 4 result from the known effect that heating (lane 3) or not heating (lane 4) has on the resolution of the MHV structural proteins (17). As anticipated, the WA3.10 MAb precipitated the S protein of MHV (lane 5) but not the FIPV S protein (lane 13). When these antibodies were used for immunoprecipitations on the mFIPV-infected cell lysates, we observed that the anti-FIPV G73 antibodies precipitated the M and N proteins but not the S protein (lane 6). The S protein was also not precipitated by the 23F4.5 MAb (lane 7) but was clearly present in the immunoprecipitate obtained with the anti-MHV serum (lane 8), as well as in the precipitate prepared with the WA3.10 MAb (lane 9). The protein appeared to comigrate with the S protein synthesized in MHV-infected cells, a finding that is consistent with its predicted size: the ectodomain replacement should have shortened the mature S protein by 126 aa to a chimeric protein of 1,309 aa, which is identical to the mature size of the MHV S protein. These results are in agreement with the genetic analysis and demonstrate that mFIPV is indeed a chimeric FIPV expressing an S protein with an MHV-derived ectodomain.

A similar conclusion could be drawn from an immunofluorescence analysis in which LR7 cells were infected with mFIPV (Fig. 5). As controls, FCWF cells infected with FIPV and LR7 cells infected with MHV were analyzed in parallel. The infected cells were fixed at 6 h p.i., permeabilized, and treated with antibodies G73 (αFIPV), 23F4.5 (αS_f), and WA3.10

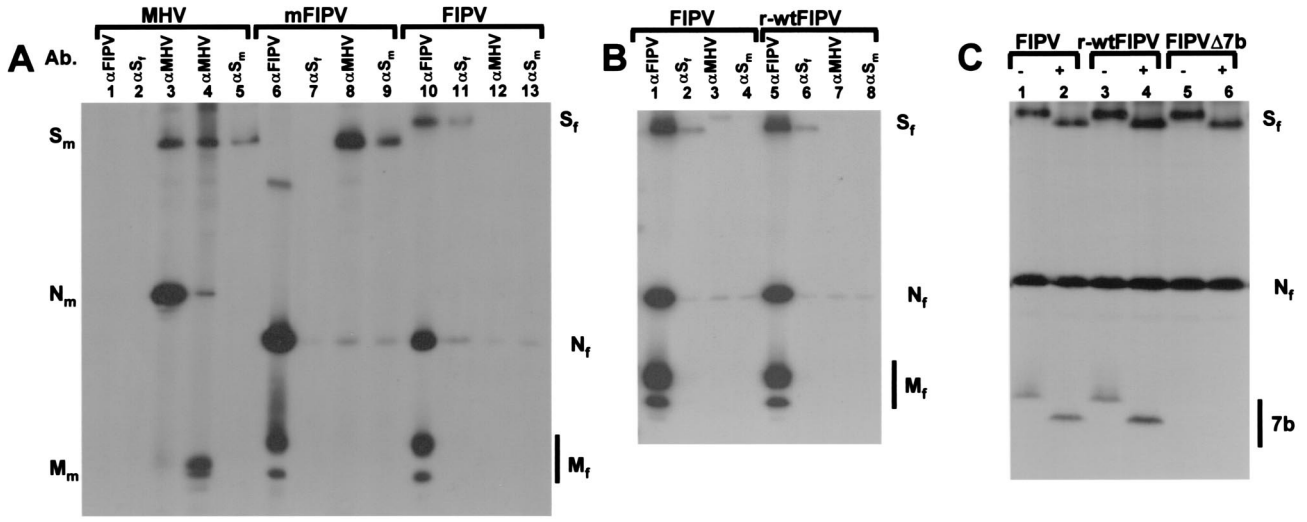

FIG. 4. Viral proteins in mFIPV-infected LR7 cells (A), in r-wtFIPV infected FCWF cells (B), and in FIPVΔ7b-infected FCWF cells (C). In panel A, analyses were done with LR7 cells infected with mFIPV and, for comparison, with MHV-infected LR7 cells and FIPV-infected FCWF cells. In panel B, analyses were done with r-wtFIPV-infected FCWF cells and, for comparison, with FIPV-infected FCWF cells, and in panel C, analyses were done with FIPVΔ7b-infected FCWF cells and, for comparison, with FIPV- and r-wtFIPV-infected FCWF cells. In all cases the cells were labeled for 2 h with ^{35}S-labeled amino acids. Immunoprecipitations were performed on aliquots of cleared lysates of these cells by using the following antibodies: ascitic fluid G73 (αFIPV) from an FIPV-infected cat; K134 (αMHV), a rabbit serum raised against purified MHV strain A59; WA3.10 (αS_m), an MAb against an epitope present in the MHV S ectodomain; and 23F4.5 (αS_f), an MAb against an epitope in the FIPV S ectodomain. All samples were heated at 95°C prior to electrophoresis, except for the sample analyzed in panel A, lane 4, which was run without heating and analyzed in sodium dodecyl sulfate–12.5% polyacrylamide gels. The positions of the S, N, M, and 7b (C) proteins are indicated at the left for MHV and at the right for FIPV.

(αS_m), respectively, and subsequently stained with fluorescent secondary antibodies. The FIPV-infected control cells showed a specific signal only when treated with the G73 (αFIPV) or 23F4.5 (αS_f) antibodies but not when treated with MAb WA3.10 (αS_m). Conversely, the former antibodies did not stain MHV-infected cells, whereas the WA3.10 MAb did (Fig. 5). Inspection of the mFIPV-infected cells revealed a specific immunofluorescence signal after treatment with antibodies G73 (αFIPV) or WA3.10 (αS_m) but not after treatment with 23F4.5 (αS_f), again demonstrating that mFIPV expresses FIPV proteins, as well as an MHV S epitope, but does not express an FIPV S epitope.

Tissue culture growth phenotype of mFIPV. Having confirmed the identity of the recombinant mFIPV genetically and immunologically, we studied its growth properties in more detail. Thus, we compared the growth kinetics of the virus in murine LR7 cells with that of MHV in these same cells and with that of the parental FIPV in feline FCWF cells. Representative one-step growth curves are shown in Fig. 6. Although the general shape of these curves was quite similar, MHV appeared to reach its peak titer slightly faster than did mFIPV (Fig. 6A). The maximal titers obtained were always some 1 to 2 log units higher for MHV than for mFIPV. Titers of up to 10^7 50% tissue culture infective doses/ml were obtained with mFIPV, a level that is comparable to the titers obtained with the wild-type FIPV grown on FCWF cells.

The cytopathic effect induced in mFIPV-infected cells was qualitatively similar to that seen in these cells after MHV infection. Many syncytia were seen developing initially that increased in number and grew more extensive during the course of the infection. However, this process started earlier in the MHV-infected cells and also clearly progressed faster. The dramatic cytopathic effects dominated by huge syncytia eventually observed after MHV infection of LR7 cells were never seen with mFIPV. Apparently, cell-cell fusion is less efficient, which might explain why mFIPV failed to produce plaques in these cells even after 72 h of incubation under a standard agar overlay.

Generation of r-wtFIPV and of a targeted FIPV mutant (FIPVΔ7b). mFIPV had been created as the key recipient virus for the future production of FIPV mutants. It was therefore of crucial importance to first recreate a (recombinant) wild-type FIPV (r-wtFIPV) and then verify that its in vitro and in vivo features were still identical to those of the original wild-type virus. With this aim, plasmid pBRDI1 was prepared (Fig. 2). In addition, we wanted to demonstrate that directed mutations can indeed be introduced into the FIPV genome. To this end, we designed the construction of a virus in which the synthesis of a nonessential gene was abolished. Thus, plasmid pBRDIΔATG7b was constructed, in which the initiation codon of the nonstructural 7b gene is mutated into GTG while, simultaneously, a *Pml*I restriction site is introduced (Fig. 7B). The 7b gene is dispensable for viral growth in vitro (50). As a negative control pBRDIΔMluI was constructed. In this plasmid the *Mlu*I restriction site is filled in with Klenow enzyme (Fig. 7D), resulting in an out-of-frame mutation in the essential nucleocapsid gene.

A recombination experiment was carried out in LR7 cells infected with mFIPV by transfecting these cells in parallel with synthetic RNA A, RNA1Δ7b, and RNAΔMluI transcripts, respectively (Fig. 1). No coculturing with FCWF cells was applied. Culture media were harvested at 24 h p.i., and the

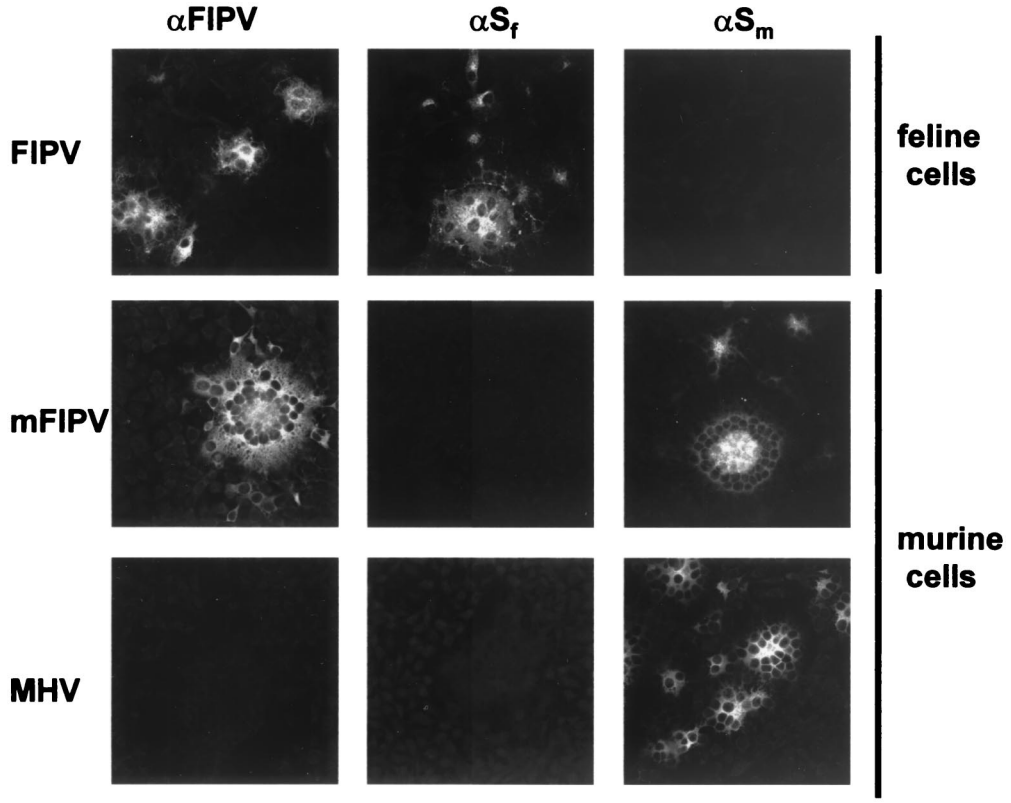

FIG. 5. Immunofluorescence analysis of mFIPV infected cells. LR7 cells were infected with mFIPV. For comparison, LR7 cells and FCWF cells were infected with MHV and FIPV, respectively. Infections were visualized at 6 h p.i. by immunofluorescence microscopy on permeabilized cells with the following antibodies: ascitic fluid G73 (αFIPV) from an FIPV-infected cat; 23F4.5 (αS$_f$), an MAb against an epitope in the FIPV S ectodomain; and WA3.10 (αS$_m$), an MAb against an epitope present in the MHV S ectodomain.

number of candidate recombinants from the three recombination assays was determined through a direct plaque assay on FCWF cells. To determine whether the desired progeny was obtained, viral RNA was isolated from several plaques and subjected to RT-PCR (Fig. 7).

The recombinations with transcripts RNA A and RNA1Δ7b yielded ca. 5×10^2 PFU/ml on FCWF cells (average of three recombination experiments). RT-PCR carried out with primers PR76 and PR1295 on RNA isolated from four plaques obtained with RNA1Δ7b progeny (FIPVΔ7b) confirmed that the desired mutation was indeed incorporated since all four viruses had acquired a *Pml*I restriction site (Fig. 7A). This result was in contrast to the r-wtFIPV's RT-PCR product, which lacked this restriction site, as expected. Using RNA1ΔMluI as the donor RNA, a considerably lower number of plaques (on average, 20 PFU/ml) was produced, which is ca. 4% the number obtained with RNA A and RNA1Δ7b. These recombinants were probably the result of double recombina-

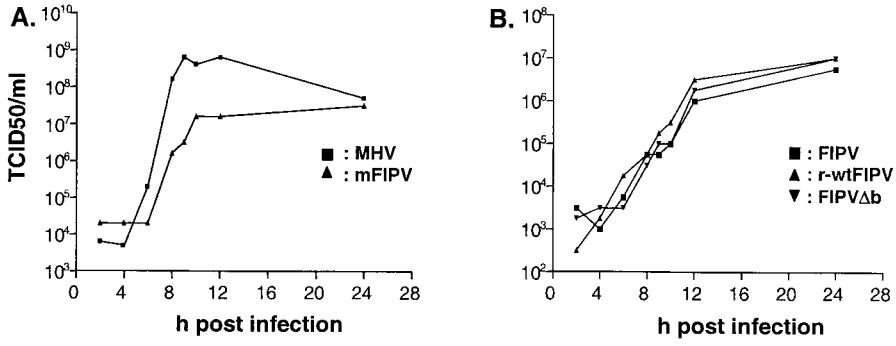

FIG. 6. Growth of mFIPV in murine cells (A) and of r-wtFIPV and FIPVΔ7b in feline cells (B). Single-step growth kinetics of mFIPV and MHV in LR7 cells (A) and of r-wtFIPV, FIPVΔ7b, and FIPV in FCWF cells (B). The viral infectivity in the culture medium was determined at different times postinfection by a quantal assay on LR7 cells or FCWF cells, and the 50% tissue culture infective doses ($TCID_{50}$) were calculated.

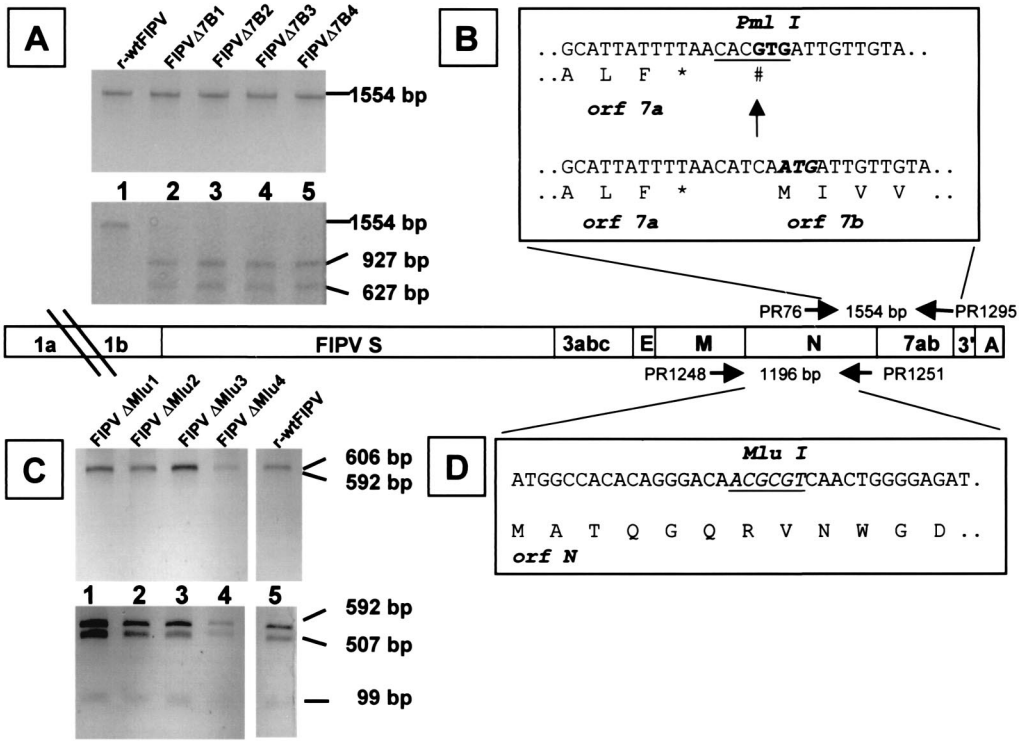

FIG. 7. RT-PCR analysis of the r-wtFIPV, FIPVΔ7b, and FIPVΔMlu recombinants. RT-PCR was used to amplify the ORF 7b region (A and B) and the N gene region (C and D) with RNA isolated from cells infected with r-wtFIPV and FIPVΔ7b (A) and with r-wtFIPV and FIPVΔMlu (C) as a template, respectively. A physical map of the FIPV genome is shown in the middle of the figure. The locations of the primers (see Table 1 for sequences) are indicated by arrows, together with the expected sizes of the PCR products predicted for the indicated primer pairs. (B) Sequence of the ORF 7ab region with the gene 7b start codon in boldface and italics (bottom) and with the introduced mutations disrupting this codon and creating a *Pml*I restriction site indicated (top, underlined). (A) RT-PCR products obtained with RNA from four independent FIPVΔ7b mutant viruses with primers PR76 and PR1295. Undigested products are at the top, and products digested with *Pml*I are at the bottom. (D) Partial sequence of the N gene with the *Mlu*I restriction site underlined. (C) RT-PCR products obtained with RNA from four independent FIPVΔMlu mutant viruses with the primers PR1248 and PR1251. Products digested with *Xba*I are at the top, and products digested with *Xba*I and *Mlu*I are at the bottom.

tion events. This was confirmed by performing RT-PCR with primers PR1248 and PR1251 on RNA isolated from four independently obtained plaques of RNA1ΔMlu progeny (Fig. 7C); each of the PCR products contained the *Mlu*I restriction site (Fig. 7C, bottom). Since the mobility difference between the undigested PCR fragment (1,198 bp) and the large fragment obtained after *Mlu*I digestion (1,099 bp) was minimal, the fragments were digested with either *Xba*I (Fig. 7C, top), which results in two fragments almost identical in size (606 and 592 bp), or both *Xba*I and *Mlu*I, resulting in fragments with the indicated sizes (Fig. 7C, bottom).

In these recombination experiments we selected the recombinant viruses straight from the LR7 cultures by direct plaque assay on FCWF cells, i.e., without amplifying these viruses by coculturing of the LR7 cells with FCWF cells. We studied the effect of coculturing on the recombinant virus yields in recombination experiments with donor RNA A and RNA1Δ7b. It appeared that coculturing with FCWF cells prior to a plaque assay resulted in much higher yields of plaques, with recombinant virus titers routinely being approximately 10^5 PFU/ml.

In vitro characteristics of r-wtFIPV and FIPVΔ7b. The in vitro phenotypes of the recombinant viruses r-wtFIPV and FIPVΔ7b were investigated in feline FCWF cells. Importantly, the growth characteristics of r-wtFIPV were indistinguishable from its parental virus FIPV 79-1146. As their one-step growth curves demonstrate, the replication kinetics and the infectivity yields of these virus strains were very similar (Fig. 6B). The same results were obtained with FIPVΔ7b (Fig. 6B).

FIPV 79-1146 induces strong cytopathic effects in FCWF cells characterized by massive syncytia. Similar effects were seen when these cells were infected with r-wtFIPV or with FIPVΔ7b. Neither recombinant virus was capable of infecting mouse LR7 cells, in contrast to their immediate precursor mFIPV. Clearly, complete reversal of host cell tropism had occurred as a result of the recombinations.

To verify that r-wtFIPV had indeed regained the FIPV S gene, FCWF cells were infected with the virus and the proteins were labeled with ^{35}S-labeled amino acids. For comparison, FCWF cells were infected with FIPV and radiolabeled in parallel. After the labeling, cell lysates were prepared and immunoprecipitations were carried out as described above with the same antibodies. The electrophoretic patterns obtained with FIPV and r-wtFIPV shown in Fig. 4B were completely identical and thus confirmed the predictions. In both cases the typical set of FIPV proteins S, M, and N was precipitated by the polyclonal anti-FIPV antibodies (lanes 1 and 5), but none of these proteins was precipitated by the polyclonal anti-MHV serum (lanes 3 and 7). Immunoprecipitations with the 23F4.5

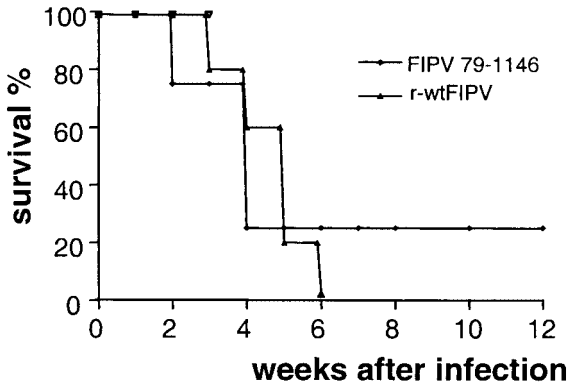

FIG. 8. In vivo survival after infection with FIPV 79-1146 and r-wtFIPV. Kittens (5 months old) were inoculated with 100 PFU of FIPV 79-1146 ($n = 4$) or r-wtFIPV ($n = 5$).

MAb (lanes 2 and 6) but not with the WA3.10 MAb (lanes 4 and 8) brought down the S protein.

To determine whether the disruption of the ATG initiation codon of the ORF 7b gene in FIPVΔ7b had resulted in a 7b protein-deficient virus, FCWF cells were infected and the proteins were labeled with [^{35}S]cysteine. Similar labelings were done in parallel with FCWF cells infected with FIPV 79-1146 and with r-wtFIPV. Cell lysates were prepared and immunoprecipitations were carried out with the G73 (αFIPV) antibodies. The samples were heated for 5 min at 95°C to aggregate the M protein (17), which otherwise migrates with approximately the same mobility as the 7b protein (49), thereby often obscuring its presence. As is clear from Fig. 4C, both FIPV 79-1146 and r-wtFIPV expressed an FIPV-specific protein with the features of the 7b protein. It migrated with an apparent molecular mass of ca. 28 kDa (lanes 1 and 3). Treatment of the immunoprecipitates with endoglycosidase F indicated that the band represented a glycoprotein since its mobility increased by ca. 2 kDa (lanes 2 and 4), a finding consistent with the removal of one oligosaccharide side chain (49). The 7b glycoprotein was lacking in the FIPVΔ7b-infected cell lysate (lanes 5 and 6), indicating that the mutation around the 7b initiation codon indeed effectively inhibited 7b gene expression. This result confirms that the 7b protein is not essential for FIPV growth in cell culture.

Virulence of r-wtFIPV. The wild-type FIPV strain 79-1146 is highly virulent, routinely causing death in 70 to 90% of cats when inoculated oronasally with a low dose (100 PFU). To determine whether r-wtFIPV had maintained its virulence, nine 5-month-old cats were placed into two groups and inoculated oronasally (100 PFU) with either FIPV strain 79-1146 ($n = 4$) or r-wtFIPV ($n = 5$). Infection with both viruses induced a rapid onset of clinical disease in all cats that was characterized by depression, anorexia, jaundice, weight loss, and leukopenia. Three out of four and five out of five cats inoculated with FIPV 79-1146 and r-wtFIPV, respectively, had to be euthanized due to advanced symptoms of FIP between weeks 2 and 6 after inoculation. The survival curves are depicted in Fig. 8, showing a similar lethality for both viruses. Postmortem examination revealed both wet (effusive) and dry (noneffusive) forms of FIP with typical pyogranulomata observed in multiple organs, particularly in the liver and the spleen. The results show that r-wtFIPV had not lost any of its virulence as a result of its two recombination events and its various passages on mouse and feline cells.

DISCUSSION

FIP is one of the most serious diseases in cats. Despite its importance, however, little is known about the molecular biology of this infection. A major obstacle has been the lack of a suitable reverse genetic system for its causative agent, FIPV. As we describe here, we have now established such a system based on targeted RNA recombination. Central to our approach was the generation of an interspecies chimeric virus, mFIPV, that carries the ectodomain of a spike protein which is derived from another coronavirus, MHV. The consequent change in host cell tropism allowed the selection of this virus by its growth in murine cells. The strategy essentially involves the use of mFIPV as the recipient virus in a reverse recombination event that results in the restoration of the spike gene, allowing the recombinant viruses to be selected in turn by their growth in feline cells. Thus, we prepared wt-rFIPV, which appeared to be indistinguishable from the parental virus—FIPV strain 79-1146—not only by its in vitro growth features but also with respect to its lethal phenotype in the natural host, the cat. Finally, to demonstrate the feasibility of our strategy for reverse genetic purposes, we introduced a mutation into the FIPV genome that effectively impaired the expression of the nonstructural 7b gene. After the groundbreaking development of the prototypic MHV system, the present work establishes the second targeted RNA recombination system for coronaviruses.

The synthetic donor RNA that we designed for our recombination system was modeled after the highly effective defective interfering (DI) RNAs that were used as donors in the MHV paradigm. Here it was estimated that frequencies of recombination increase by some orders of magnitude by using a coreplicating RNA rather than a subgenomic RNA (29). DI RNAs are quite ubiquitous among nidoviruses, their occurrence having been demonstrated for all groups of coronaviruses (including TGEV [31] and MHV [27]), for BCV (4), for IBV (41), and for the Berne torovirus (45), as well as for the equine arterivirus (32). Remarkably, however, no naturally occurring DI has thus far been observed for FIPV. Although we did not confirm whether our synthetic donor RNA was actually replicated in (m)FIPV-infected cells, our recombinant virus yields support this assumption. We routinely observed 10^2 to 10^3 recombinants per 5×10^6 infected or transfected cells. Our analyses with the donor RNA carrying a lethal mutation in the N gene also showed that a substantial fraction (~4%) of our recombinant viruses had apparently been generated by double crossovers. Clearly, the FIPV system is recombinogenic as had already been made clear by the emergence of serotype II feline coronaviruses through the recombination of feline and canine coronaviruses (18, 33). Generally, the particular mode of replication and the huge genome size of coronaviruses are thought to favor polymerase template switching, thereby resulting in a remarkably high recombination rate (for a review, see reference 24).

The power of the reverse genetics strategy that we estab-

lished for FIPV lies in the ease and efficiency with which recombinant viruses are selected from the pool of progeny viruses resulting from a recombination trial. The distinctive receptor specificities of coronaviruses allowed the design of a selection principle based on the switch of host cell specificity that accompanies the exchange of different spike ectodomain sequences. Coronavirus spikes are trimeric assemblies (11) that are incorporated into viral particles by interactions with the M protein (10, 37, 40). Sequences in both the transmembrane and the endodomain of the spike protein are responsible for this interaction (B. J. Bosch and P. J. M. Rottier, unpublished data). It appeared that the swapping of ectodomains between different coronavirus S proteins was tolerated without an apparent loss of biological features (17). Thus, chimeric spikes with FIPV- and MHV-derived ectodomains were incorporated into otherwise MHV- and FIPV-based virus-like particles, respectively (17). These observations were subsequently instrumental for the generation of the chimeric viruses fMHV (22) and mFIPV that form the basis of the respective reverse genetics systems for these viruses.

Although the genetic exchange did not affect the replication of the recombinant mFIPV to a great extent, it did result in a slower formation of syncytia and the inability to produce plaques in LR7 monolayer cultures. The latter might be explained by the strongly reduced cleavage efficiency of the chimeric S protein compared to the MHV S protein (17). Inhibition of this cleavage does not affect MHV's specific infectivity, but it clearly reduces the cell-to-cell fusion caused by the spike protein that gives rise to syncytia and plaque formation (K. Stadler, G. Godeke, and P. J. M. Rottier, unpublished data).

The disruption of the initiation codon of ORF 7b abolished the expression of this gene product. The 7b polypeptide is a soluble glycosylated protein, antibodies against which are induced in infected cats (49). It is a secretory glycoprotein that presumably functions extracellularly. Deletions in the 7b gene readily occur upon propagation of FIPV in tissue culture cells. Sequence observations suggest that deletions in ORF 7b are associated with loss of virulence (19, 49, 50). Our reverse genetics system will now allow us to investigate the functions of this and other gene products in great detail. The demonstration that the wild-type FIPV strain 79-1146 that we recreated in our recombination system had fully maintained its phenotype is obviously an essential basis for such experiments.

Targeted RNA recombination offers a very convenient general strategy for the genetic manipulation of coronaviruses. The approach had so far been applied only to MHV, except for one case in which Sanchez et al. (44) demonstrated a role for the TGEV spike protein in pathogenesis. The MHV recombination system has already shown its usefulness for the study of aspects as diverse as virus assembly (8, 9, 15, 23), transcription and replication (14, 20, 21), and tropism and virulence (22, 25, 26, 35, 36, 39, 42) and for the development of coronaviruses as vectors (14; C. A. M. de Haan, B. J. Haijema, H. Volders, and P. J. M. Rottier, unpublished data). When compared to the different full-size infectious cDNA clones that were recently described for TGEV (1, 51), HuCV (46), IBV (2), and MHV (52), targeted RNA recombination systems based on interspecies chimeric viruses such as mFIPV and fMHV obviously have attractive technical advantages for the engineering of coronavirus genomes. The most important of these advantages are the easier manipulation of the smaller, subgenomic cDNA donor constructs used, the high efficiency of homologous recombination, and the extremely simple selection of the recombinant viruses. There are, however, clear limitations. One is the inherent inability to study lethal mutations due to the requirement for passaging, a limitation not met with infectious cDNA clones which in principle allow such mutations to be analyzed in a single round of infection. Another limitation is associated with the limited genomic segment, i.e., the domain downstream of the ORF 1b gene, that is accessible for manipulation by the targeted recombination systems, as opposed to the entire virus genome that can be covered by infectious cDNA clones. Although there is no solution to the first problem, the second limitation is not as dramatic as it seems since it still allows the manipulation of all but one of the coronaviral genes, including all intergenic regions and the 3′ noncoding region.

ACKNOWLEDGMENTS

We thank Martin Raamsman and Hao Yun Wong for assistance with part of the experimental work, Herman Egberink for excellent help with the animal studies, Harry Vennema and Raoul de Groot for constructive support, and Marian Horzinek for careful reading of the manuscript.

This work was supported by financial aid from The Netherlands Organization for Scientific Research and Netherlands Foundation for Applied Sciences to B.J.H. and H.V.

REFERENCES

1. **Almazan, F., J. M. Gonzalez, Z. Penzes, A. Izeta, E. Calvo, J. Plana-Duran, and L. Enjuanes.** 2000. Engineering the largest RNA virus genome as an infectious bacterial artificial chromosome. Proc. Natl. Acad. Sci. USA **97:** 5516–5521.
2. **Casais, R., V. Thiel, S. G. Siddell, D. Cavanagh, and P. Britton.** 2001. Reverse genetics system for the avian coronavirus infectious bronchitis virus. J. Virol. **75:**12359–12369.
3. **Cavanagh, D.** 1995. The coronavirus surface protein, p. 73–103. *In* S. G. Siddell (ed.), The *Coronaviridae*. Plenum Press, Inc., New York, N.Y.
4. **Chang, R. Y., M. A. Hofmann, P. B. Sethna, and D. A. Brian.** 1994. A *cis*-acting function for the coronavirus leader in defective interfering RNA replication. J. Virol. **68:**8223–8231.
5. **de Groot, R. J., A. C. Andeweg, M. C. Horzinek, and W. J. Spaan.** 1988. Sequence analysis of the 3′ end of the feline coronavirus FIPV 79–1146 genome: comparison with the genome of porcine coronavirus TGEV reveals large insertions. Virology **167:**370–376.
6. **de Groot, R. J., J. A. Lenstra, W. Luytjes, H. G. Niesters, M. C. Horzinek, B. A. van der Zeijst, and W. J. Spaan.** 1987. Sequence and structure of the coronavirus peplomer protein. Adv. Exp. Med. Biol. **218:**31–38.
7. **de Groot, R. J. H., and M. C. Horzinek.** 1995. Feline infectious peritonitis, p. 293–309. *In* S. G. Siddell (ed.), The *Coronaviridae*. Plenum Press, Inc., New York, N.Y.
8. **de Haan, C. A., M. de Wit, L. Kuo, C. Montalto, P. S. Masters, S. R. Weiss, and P. J. Rottier.** 2002. O-glycosylation of the mouse hepatitis coronavirus membrane protein. Virus Res. **82:**77–81.
9. **de Haan, C. A., L. Kuo, P. S. Masters, H. Vennema, and P. J. Rottier.** 1998. Coronavirus particle assembly: primary structure requirements of the membrane protein. J. Virol. **72:**6838–6850.
10. **de Haan, C. A., M. Smeets, F. Vernooij, H. Vennema, and P. J. Rottier.** 1999. Mapping of the coronavirus membrane protein domains involved in interaction with the spike protein. J. Virol. **73:**7441–7452.
11. **Delmas, B., and H. Laude.** 1990. Assembly of coronavirus spike protein into trimers and its role in epitope expression. J. Virol. **64:**5367–5375.
12. **de Vries, A. A. F. H., M. C. Horzinek, P. J. M. Rottier, and R. J. de Groot.** 1997. The genome organization of the *Nidovirales*: similarities and differences between arteri-, toro-, and coronaviruses. Semin. Virol. **8:**33–47.
13. **Escors, D., J. Ortego, H. Laude, and L. Enjuanes.** 2001. The membrane M protein carboxy terminus binds to transmissible gastroenteritis coronavirus core and contributes to core stability. J. Virol. **75:**1312–1324.
14. **Fischer, F., C. F. Stegen, C. A. Koetzner, and P. S. Masters.** 1997. Analysis of a recombinant mouse hepatitis virus expressing a foreign gene reveals a novel aspect of coronavirus transcription. J. Virol. **71:**5148–5160.
15. **Fischer, F., C. F. Stegen, P. S. Masters, and W. A. Samsonoff.** 1998. Analysis of constructed E gene mutants of mouse hepatitis virus confirms a pivotal role for E protein in coronavirus assembly. J. Virol. **72:**7885–7894.

16. **Glaser, A. L., A. A. F. de Vries, M. J. B. Raamsman, M. C. Horzinek, and P. J. M. Rottier.** 1999. An infectious cDNA clone of equine arteritis virus: a tool for for future fundamental studies and vaccine development, p. 166–176. *In* W. R. Plowright, P. D. Rossdale, and J. F. Wade (ed.), Proceedings of the 8th International Conference on Equine Infectious Diseases, Dubai 1998. R&W Publications, Newmarket, United Kingdom.
17. **Godeke, G. J., C. A. de Haan, J. W. Rossen, H. Vennema, and P. J. Rottier.** 2000. Assembly of spikes into coronavirus particles is mediated by the carboxy-terminal domain of the spike protein. J. Virol. **74:**1566–1571.
18. **Herrewegh, A. A., I. Smeenk, M. C. Horzinek, P. J. Rottier, and R. J. de Groot.** 1998. Feline coronavirus type II strains 79–1683 and 79–1146 originate from a double recombination between feline coronavirus type I and canine coronavirus. J. Virol. **72:**4508–4514.
19. **Herrewegh, A. A., H. Vennema, M. C. Horzinek, P. J. Rottier, and R. J. de Groot.** 1995. The molecular genetics of feline coronaviruses: comparative sequence analysis of the ORF7a/7b transcription unit of different biotypes. Virology **212:**622–631.
20. **Hsue, B., T. Hartshorne, and P. S. Masters.** 2000. Characterization of an essential RNA secondary structure in the 3′ untranslated region of the murine coronavirus genome. J. Virol. **74:**6911–6921.
21. **Hsue, B., and P. S. Masters.** 1997. A bulged stem-loop structure in the 3′ untranslated region of the genome of the coronavirus mouse hepatitis virus is essential for replication. J. Virol. **71:**7567–7578.
22. **Kuo, L., G. J. Godeke, M. J. Raamsman, P. S. Masters, and P. J. Rottier.** 2000. Retargeting of coronavirus by substitution of the spike glycoprotein ectodomain: crossing the host cell species barrier. J. Virol. **74:**1393–1406.
23. **Kuo, L., and P. S. Masters.** 2002. Genetic evidence for a structural interaction between the carboxy termini of the membrane and nucleocapsid proteins of mouse hepatitis virus. J. Virol. **76:**4987–4999.
24. **Lai, M. M. C.** 1996. Recombination in large RNA viruses: coronaviruses. Semin. Virol. **7:**381–388.
25. **Lavi, E., L. Kuo, J. A. Haluskey, and P. S. Masters.** 1998. Targeted recombination between MHV-2 and MHV-A59 to study neurotropic determinants of MHV. Adv. Exp. Med. Biol. **440:**543–547.
26. **Leparc-Goffart, I., S. T. Hingley, M. M. Chua, J. Phillips, E. Lavi, and S. R. Weiss.** 1998. Targeted recombination within the spike gene of murine coronavirus mouse hepatitis virus-A59: Q159 is a determinant of hepatotropism. J. Virol. **72:**9628–9636.
27. **Makino, S., C. K. Shieh, L. H. Soe, S. C. Baker, and M. M. Lai.** 1988. Primary structure and translation of a defective interfering RNA of murine coronavirus. Virology **166:**550–560.
28. **Masters, P. S.** 1999. Reverse genetics of the largest RNA viruses. Adv. Virus Res. **53:**245–264.
29. **Masters, P. S., C. A. Koetzner, C. A. Kerr, and Y. Heo.** 1994. Optimization of targeted RNA recombination and mapping of a novel nucleocapsid gene mutation in the coronavirus mouse hepatitis virus. J. Virol. **68:**328–337.
30. **McKeirnan, A. J., J. F. Evermann, A. Hargis, L. M. Miller, and R. L. Ott.** 1981. Isolation of feline coronaviruses from two cats with diverse disease manifestations. Feline Prac. **11:**16–20.
31. **Mendez, A., C. Smerdou, A. Izeta, F. Gebauer, and L. Enjuanes.** 1996. Molecular characterization of transmissible gastroenteritis coronavirus defective interfering genomes: packaging and heterogeneity. Virology **217:**495–507.
32. **Molenkamp, R., B. C. Rozier, S. Greve, W. J. Spaan, and E. J. Snijder.** 2000. Isolation and characterization of an arterivirus defective interfering RNA genome. J. Virol. **74:**3156–3165.
33. **Motokawa, K., T. Hohdatsu, H. Hashimoto, and H. Koyama.** 1996. Comparison of the amino acid sequence and phylogenetic analysis of the peplomer, integral membrane and nucleocapsid proteins of feline, canine, and porcine coronaviruses. Microbiol. Immunol. **40:**425–433.
34. **Narayanan, K., and S. Makino.** 2001. Cooperation of an RNA packaging signal and a viral envelope protein in coronavirus RNA packaging. J. Virol. **75:**9059–9067.
35. **Navas, S., S. H. Seo, M. M. Chua, J. Das Sarma, S. T. Hingley, E. Lavi, and S. R. Weiss.** 2001. Role of the spike protein in murine coronavirus-induced hepatitis: an in vivo study using targeted RNA recombination. Adv. Exp. Med. Biol. **494:**139–144.
36. **Navas, S., S. H. Seo, M. M. Chua, J. D. Sarma, E. Lavi, S. T. Hingley, and S. R. Weiss.** 2001. Murine coronavirus spike protein determines the ability of the virus to replicate in the liver and cause hepatitis. J. Virol. **75:**2452–2457.
37. **Nguyen, V. P., and B. G. Hogue.** 1997. Protein interactions during coronavirus assembly. J. Virol. **71:**9278–9284.
38. **Olsen, C. W., W. V. Corapi, C. K. Ngichabe, J. D. Baines, and F. W. Scott.** 1992. Monoclonal antibodies to the spike protein of feline infectious peritonitis virus mediate antibody-dependent enhancement of infection of feline macrophages. J. Virol. **66:**956–965.
39. **Ontiveros, E., L. Kuo, P. S. Masters, and S. Perlman.** 2001. Inactivation of expression of gene 4 of mouse hepatitis virus strain JHM does not affect virulence in the murine CNS. Virology **289:**230–238.
40. **Opstelten, D. J., M. J. Raamsman, K. Wolfs, M. C. Horzinek, and P. J. Rottier.** 1995. Envelope glycoprotein interactions in coronavirus assembly. J. Cell Biol. **131:**339–349.
41. **Penzes, Z., K. Tibbles, K. Shaw, P. Britton, T. D. Brown, and D. Cavanagh.** 1994. Characterization of a replicating and packaged defective RNA of avian coronavirus infectious bronchitis virus. Virology **203:**286–293.
42. **Phillips, J. J., M. M. Chua, E. Lavi, and S. R. Weiss.** 1999. Pathogenesis of chimeric MHV4/MHV-A59 recombinant viruses: the murine coronavirus spike protein is a major determinant of neurovirulence. J. Virol. **73:**7752–7760.
43. **Rottier, P. J., W. J. Spaan, M. C. Horzinek, and B. A. van der Zeijst.** 1981. Translation of three mouse hepatitis virus strain A59 subgenomic RNAs in *Xenopus laevis* oocytes. J. Virol. **38:**20–26.
44. **Sanchez, C. M., A. Izeta, J. M. Sanchez-Morgado, S. Alonso, I. Sola, M. Balasch, J. Plana-Duran, and L. Enjuanes.** 1999. Targeted recombination demonstrates that the spike gene of transmissible gastroenteritis coronavirus is a determinant of its enteric tropism and virulence. J. Virol. **73:**7607–7618.
45. **Snijder, E. J., J. A. den Boon, M. C. Horzinek, and W. J. Spaan.** 1991. Characterization of defective interfering RNAs of Berne virus. J. Gen. Virol. **72:**1635–1643.
46. **Thiel, V., J. Herold, B. Schelle, and S. G. Siddell.** 2001. Infectious RNA transcribed in vitro from a cDNA copy of the human coronavirus genome cloned in vaccinia virus. J. Gen. Virol. **82:**1273–1281.
47. **van der Most, R. G. A. S., and W. J. M. Spaan.** 1995. Coronavirus replication, transcription, and RNA recombination, p. 11–31. Plenum Press, London, United Kingdom.
48. **Vennema, H., G. J. Godeke, J. W. Rossen, W. F. Voorhout, M. C. Horzinek, D. J. Opstelten, and P. J. Rottier.** 1996. Nucleocapsid-independent assembly of coronavirus-like particles by co-expression of viral envelope protein genes. EMBO J. **15:**2020–2028.
49. **Vennema, H., L. Heijnen, P. J. Rottier, M. C. Horzinek, and W. J. Spaan.** 1992. A novel glycoprotein of feline infectious peritonitis coronavirus contains a KDEL-like endoplasmic reticulum retention signal. J. Virol. **66:**4951–4956.
50. **Vennema, H., J. W. Rossen, J. Wesseling, M. C. Horzinek, and P. J. Rottier.** 1992. Genomic organization and expression of the 3′ end of the canine and feline enteric coronaviruses. Virology **191:**134–140.
51. **Yount, B., K. M. Curtis, and R. S. Baric.** 2000. Strategy for systematic assembly of large RNA and DNA genomes: transmissible gastroenteritis virus model. J. Virol. **74:**10600–10611.
52. **Yount, B., M. R. Denison, S. R. Weiss, and R. S. Baric.** 2002. Systematic assembly of a full-length infectious cDNA of mouse hepatitis virus strain A59. J. Virol. **76:**11065–11078.